Featured in Physics

Chiral Domain Structure in Superfluid ^{3}He-*A* Studied by Magnetic Resonance Imaging

J. Kasai,[1] Y. Okamoto,[1] K. Nishioka,[1] T. Takagi,[3] and Y. Sasaki[1,2,*]
[1]*Department of Physics, Graduate School of Science, Kyoto University, Kitashirakawa-Oiwake-Cho, Sakyo-ku, Kyoto 606-8502, Japan*
[2]*Research Center for Low Temperature and Materials Sciences, Kyoto University, Yoshida-honmachi, Sakyo-ku, Kyoto 606-8501, Japan*
[3]*Department of Applied Physics, University of Fukui, Bunkyo 3-9-1, Fukui 910-8507, Japan*

(Received 18 September 2017; revised manuscript received 5 December 2017; published 17 May 2018)

The existence of a spatially varying texture in superfluid ^{3}He is a direct manifestation of the complex macroscopic wave function. The real space shape of the texture, namely, a macroscopic wave function, has been studied extensively with the help of theoretical modeling but has never been directly observed experimentally with spatial resolution. We have succeeded in visualizing the texture by a specialized magnetic resonance imaging. With this new technology, we have discovered that the macroscopic chiral domains, of which sizes are as large as 1 mm, and corresponding chiral domain walls exist rather stably in ^{3}He-*A* film at temperatures far below the transition temperature.

DOI: 10.1103/PhysRevLett.120.205301

Modern interest in topological superfluids and superconductors has revived the significance of superfluid ^{3}He because of the most precisely understood macroscopic wave function of triplet *p* wave BCS superfluids. The topological nature of these quantum materials appears in connection to the boundary condition at the border and interface of the material. For a precise study on the topological properties, it is important to control the boundary conditions of the materials. The extremely precise understanding of the macroscopic wave function and its controllability of boundary conditions in real experimental situations makes superfluid ^{3}He an outstandingly suitable system for studying topological superfluids and superconductors. Specifically, the *A* phase of superfluid ^{3}He is regarded as a chiral superfluid because of the macroscopically aligned orbital angular momentum of its Cooper pairs [1,2]. Walmsley and Golov [3] were the first to show the existence of a macroscopically aligned orbital angular momentum in a thin slab of ^{3}He-*A* by using a torsional oscillator measurement in combination with a rotating ultralow temperature cryostat. Later, Ikegami *et al.* [4,5] obtained direct evidence of a bistability in the effect of the intrinsic Magnus force on electron transport in the vicinity of the free surface of a ^{3}He-*A* film. They also observed metastable intermediate states, which suggest the existence of a multidomain structure of macroscopically aligned orbital angular momentum. The proposed multidomain structure is nothing other than a chiral domain structure, consisting of macroscopic domains of monochirality and chiral domain walls between domains of opposite chirality. Naive consideration suggests the stability of a monochirality single domain structure because of the extra energy cost due to domain walls. As is discussed for the case of a *p* wave superconductor [6], a mesoscopic sample might have a multichiral domain structure. Some of the experimental studies on the possible chiral superconductor Sr_2RuO_4 [7,8] have suggested the existence of a multichiral domain structure. The results indicated the existence of a chiral domain wall that separates the domains with opposite chirality. Walmsley *et al.* [9,10] also suggested the existence of domain walls in their torsional oscillator study to explain the observed low critical velocity of vortex penetration. However, the macroscopic shape and location of the wall and how it is stabilized are still far out of the reach of the researchers. The observed metastable state of the multiple domain structure in a ^{3}He-*A* film is probably made of macroscopic domains, which appeared accidentally due to multiple nucleation. However, if there is a condition in which a multichiral domain structure is stabilized, it would be quite useful in studying various long-standing problems, such as the existence of an edge mass current at the chiral domain wall and the existence of macroscopic intrinsic angular momentum [11].

The symmetry of order parameter in ^{3}He-*A* is described by two unit vectors $\hat{\boldsymbol{d}}$ which represent the anisotropic axis in spin space and $\hat{\boldsymbol{l}}$ which represents the axis of orbital angular momentum of a Cooper pair. Together with the indispensable orientation effect on $\hat{\boldsymbol{l}}$ at the surface, much smaller anisotropic energies such as dipole energy and magnetic anisotropy energy affect the orientation of $\hat{\boldsymbol{l}}$ and $\hat{\boldsymbol{d}}$. In addition to these orientation energies, gradient energies prevent a short-range spatial variation of $\hat{\boldsymbol{d}}$ and $\hat{\boldsymbol{l}}$. The orientations of $\hat{\boldsymbol{d}}$ and $\hat{\boldsymbol{l}}$, which favor each energy, are often contradictory to each other. Thus, the ground state texture is

 © 2018 American Physical Society

determined such that the total free energy is minimized. In bulk ^{3}He-A, the ground state has a uniform texture, $\hat{\boldsymbol{l}} \| \hat{\boldsymbol{d}} \perp \boldsymbol{H}$.

Nuclear magnetic resonance (NMR) provides very useful information for studying the texture in superfluid ^{3}He. The resonance frequency ω is shifted from the Larmor frequency ω_L as $\omega^2 = \omega_L^2 + R_T^2 \Omega_A^2$, where Ω_A represents the magnitude of a dipolar frequency shift. The normalized frequency shift R_T^2 varies from -1 to $+1$ depending on the texture in most cases. For the ground state uniform texture in bulk, R_T^2 should be unity. In the general case, motion of the spin is expressed as an eigenfunction of a Schrödinger-like equation inside a potential, which represents the shape of a nonuniform texture. An eigenvalue of the equation corresponds to the R_T^2. The eigenfunction for a uniform texture represents a uniform motion in the entire space. However, a localized spin wave mode may appear where the texture varies in space. In many cases, the frequency of a spin wave mode localized around a topological defect is different from the frequency of the bulk material. Thus, the presence of a satellite resonance peak indicates the existence of a topological defect. The type of topological defect can be determined through comparisons between the observed satellite frequency and numerical estimations of the localized spin wave mode based on the numerical modeling of topological defects. This method has been quite successful in the sense that many kinds of topological defects, such as quantized vortices [12–17] and textural solitons [18], have been identified. However, no method has been developed to observe the real space shape and locations of the defect without relying on the model.

We have succeeded in developing a magnetic resonance imaging (MRI) technique [19] that is specialized to study quantum condensate at micro Kelvin temperatures. MRI is an advanced form of NMR, which makes use of linear magnetic field gradients in addition to the homogeneous magnetic field used for standard NMR measurements. With our latest technology, which we call magnetic resonance spectroscopic imaging (MRSI), we can obtain the NMR signal intensity and resonance frequency within the sensing area of the NMR detection coil with spatial resolution of approximately 10 μm $\times$ 10 μm for the case of 2D projection imaging. The measured spatial distribution of the resonance frequency provides the locations and shapes of magnetically distinctive textural objects in superfluid ^{3}He.

We have studied textures in superfluid ^{3}He-A contained in a single 100 μm thick slab-shaped cell, whose surface is located in parallel to the vertical z axis and horizontal x axis and is located in perpendicular to another horizontal y axis [20]. The vertical height of the slab-shaped channel is 2 mm. A NMR detecting solenoid coil, with a length of 2 mm, was wound outside the cell in the middle of the channel so that a central part of the channel, approximately 4 mm in horizontal length along x axis, can be studied. Figures 1(a) and 1(b) show MRI images obtained from normal liquid ^{3}He contained in the slab. The pressure of the

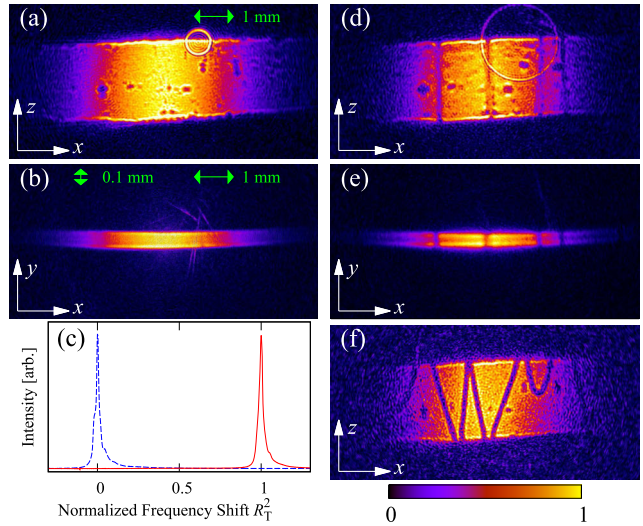

FIG. 1. Images obtained from the slab-shaped cell. MRI images in the normal phase, (a) projection to x-z plane and (b) projection to x-y plane, where the scale in the y axis is expanded by a factor of four. Colors in the images represent the intensity of the NMR signal, as indicated by the color bar. (c) NMR spectrum in the normal (broken line) and A phase (solid line) under homogeneous magnetic field. (d),(e) Images in the A phase at $T = 2.00$ mK. Thick lines along the z (y) axis in x-z (x-y) projection represent planar defects. (f) Image soon after cooling through T_C without the annealing process.

liquid ^{3}He is 2.8 MPa. Image (a) represents an x-z projection along a direction of slab thickness, namely, the y axis. Image (b) represents an x-y projection along the z axis, which is in parallel to the surface of the slab. Note that the scale in the y axis is expanded by a factor of four for easier visibility. The colors in the images indicate the NMR signal intensity originating from each location in the image. The colored beltlike shapes in the images represent the shape of the slab and the spatial distribution of the NMR sensitivity along the x axis. Visible dark spots in the x-z projection should be ignored; these are generated by magnetic broadening caused by tiny magnetic darts on the inner surface of the epoxy. A bright circle located near the top right corner of the colored beltlike shape in the x-z projection should also be ignored; this is an artifact generated by instrumental noise.

While cooling through a superfluid transition temperature $T_C = 2.41$ mK, the NMR spectrum under a homogeneous magnetic field shows almost a uniform frequency shift, which is expected for a slab geometry with a parallel magnetic field, as shown in Fig. 1(c). Figures 1(d) and 1(e) show MRI images obtained from superfluid ^{3}He-A in the slab at a temperature $T = 2.00$ mK. Since a static magnetic field for NMR is applied along the z axis, the ground state texture is expected to be the one with $\hat{\boldsymbol{d}} \| \hat{\boldsymbol{l}} \| \hat{\boldsymbol{y}}$ in the A phase. Note that four states $(\hat{\boldsymbol{d}}, \hat{\boldsymbol{l}}) = (\pm\hat{\boldsymbol{y}}, \pm\hat{\boldsymbol{y}})$ are energetically degenerate. A MRI image obtained from the uniform

ground state should look the same as that from the normal phase because of the uniform frequency shift. However, as shown in Figs. 1(d) and 1(e), several dark lines appeared in addition to the beltlike shape. The dark lines appear in different locations for each independent cooling through T_C. The lines are stable and immobile in the deep A phase at $T = 2.00$ mK. As can be seen in Figs. 1(d) and 1(e), each line appears in the same location along the x axis in both x-z and x-y projections. Thus, they are considered as a planar object extended in parallel to the y-z plane. Visible dark spots and the bright circle in the x-z projection should be ignored as stated above. We should also note that images like Figs. 1(d) and 1(e) are obtained after reshaping the irregular texture as shown in Fig. 1(f) through the annealing process, which is described later.

To further investigate the physical origin of the lines in the MRI images, we performed a much elaborated MRSI measurement on the same sample for the MRI images in Figs. 1(d) and 1(e). Figure 2 shows the local spectra extracted from the MRSI measurement and the corresponding MRSI x-z projection of the frequency component at $R_T^2 = 0.95$ to 1.05. The location of the central dark line in (b) agrees with that in the MRI images in Figs. 1(d) and 1(e). Each local spectrum shown in Fig. 2(a) represents an adjacent strip 38 μm in width in the x-coordinate. Distributions along the y and z axes are integrated. Local

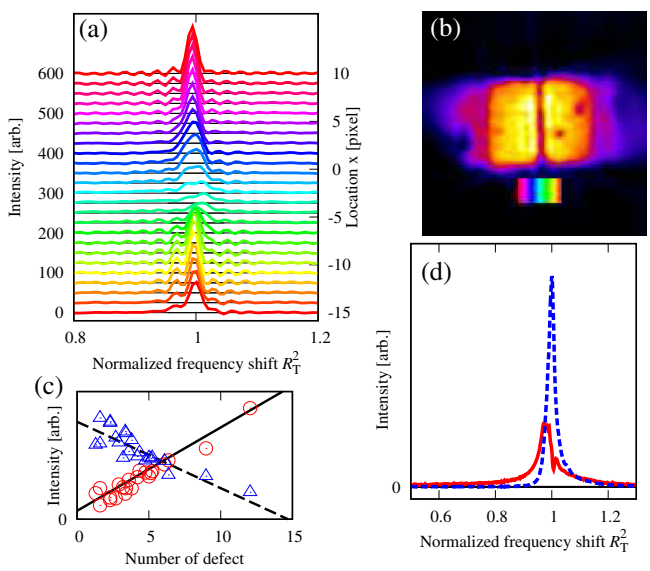

FIG. 2. MRSI data and extracted spectrum of the planar textural defect. (a) Local spectra extracted from MRSI measurements, and (b) the corresponding MRSI x-z projection of the frequency component at $R_T^2 = 0.95$ to 1.05. The color bar in (b) indicates the x coordinate of each colored spectrum in (a), which represents an adjacent strip with 38 μm (= 1 pixel) width in the x coordinate. (c) Linear dependence of spectrum height at $R_T^2 = 0.90$ (circle) and $R_T^2 = 1.00$ (triangle) on number of defects. (d) Extracted spectrum of the planar defect (solid line) and the spectrum of the uniform texture (broken line).

spectra are clearly broadened near the defect. Simultaneously, the central frequency remains nearly the same at $R_T^2 = 1$. These local NMR properties explain why the lines appear in the MRI image: localized line broadening at the planar object generates a weaker signal intensity at the corresponding location in the MRI image. We also find that the NMR spectrum in the A phase under a homogeneous magnetic field is slightly broadened towards the lower frequency from the main peak of the spectrum, together with the uniform frequency shift. The A phase spectra, obtained from various samples with different numbers of defects at $T = 2.00$ mK, have shown a positive linear dependence of spectrum height at a frequency apart from $R_T^2 = 1.00$ against the total length of the defect lines in the x-z projection, as indicated in Fig. 2(c). Negative linear dependence of the spectrum height at a frequency near $R_T^2 = 1.00$ against the total length of the defect lines in the x-z projection is shown in Fig. 2(c) as well. The linear dependence allowed us to extract the spectrum that originates from the planar defect, as shown in Fig. 2(d) [20]. The normalized frequency shift R_T^2 is slightly smaller than unity, and the linewidth is approximately a factor of two enhanced from the surroundings.

The existence of a planar textural defect in bulk ^{3}He-A was proposed by Maki and Kumar [25–27] in understanding experimental observations of a satellite peak in the NMR spectrum [18,28]. The proposed composite soliton, which has a dipole-unlocked unidirectional structure of rotating $\hat{\boldsymbol{d}}$ and $\hat{\boldsymbol{l}}$ between domains of $\hat{\boldsymbol{d}} = +\hat{\boldsymbol{l}}$ and $\hat{\boldsymbol{d}} = -\hat{\boldsymbol{l}}$, produces a satellite peak at the corresponding frequency in the NMR spectrum. A similar dipole-unlocked soliton structure, slightly modified in the constraint of the slab-shaped cell, is estimated to hold a satellite peak at $R_T^2 = 0.46, 0.66$. Since the observed NMR spectrum in our slab of ^{3}He-A has no satellite peak besides a sharp main peak at $R_T^2 = 1$, the dipole-unlocked soliton cannot be the cause of the dark lines in the MRI images. We should also note that we were able to create the dipole-unlocked solitons with a satellite peak at $R_T^2 = 0.67$, as shown in Fig. 3(a), by sending a large tipping angle excitation pulse following the method of the past experiment [18]. MRSI images in Figs. 3(b)–3(f) have complicated structures because of the formation of the soliton lattice. The dipole-unlocked solitons are located in left-hand side of the image (c), while the same kinds of solitons, as shown in Fig. 2, are located in right-hand side of the image (e). The latter remained from the initial state and were pushed toward the right during the formation of the dipole-unlocked solitons in the central region of the slab, where the tipping angle of the excitation pulse exceeds the threshold value of formation.

We made a number of cooling cycles through T_C and found that a clean A phase texture, which contains no visible defects, never appeared. The number of defects and

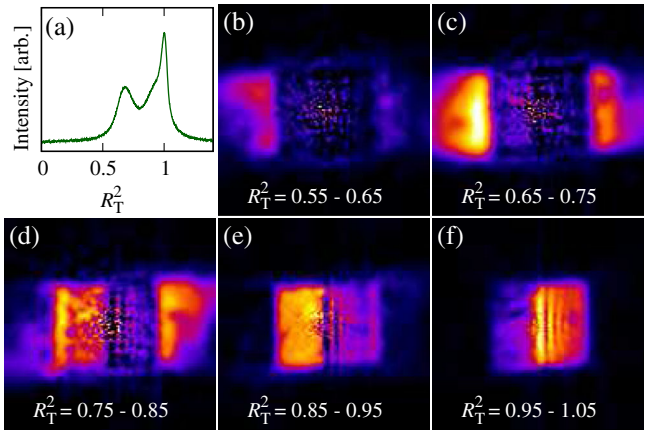

FIG. 3. Spectrum with satellite peak from dipole unlocked soliton and its MRSI images. (a) Spectrum with dipole unlocked soliton. (b)–(f) Corresponding MRSI x-z projections of the frequency component at each range of R_T^2.

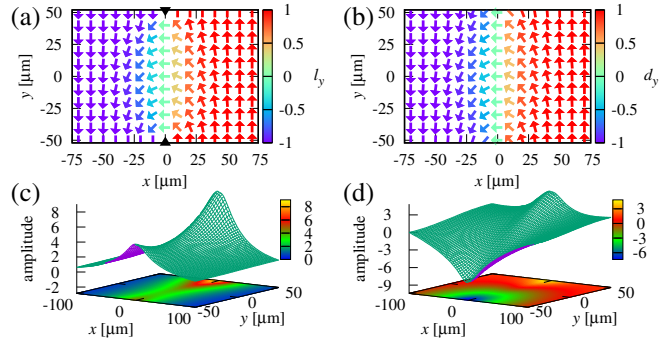

FIG. 4. Texture and standing spin wave mode of a dipole-locked soliton (DLS). (a) The $\hat{\boldsymbol{l}}$ texture and (b) $\hat{\boldsymbol{d}}$ texture of a DLS in the x-y plane, (c) the standing spin wave modes for $R_T^2 = 0.94$, and (d) for $R_T^2 = 1.02$. Triangles in (a) indicate the location of surface chiral domain walls which stabilize the DLS structure.

the location of defects changed from cooling cycle to cooling cycle. The location of defects distributed more or less evenly within the eyesight of the MRI measurement. However, the defects could persist unchanged as long as the sample was kept in the A phase at $T = 2.0$ mK, which is far below T_C. On the contrary, the number of defects could be reduced if the superfluid was warmed to temperatures near T_C, as high as $T/T_C > 0.98$. The spatial distribution of defects could also be altered during the temperature cycling process, which we call "annealing." Before annealing, curved defects, as shown in Fig. 1(f), were often observed. However, after the annealing process, we observed straight lines, as shown in Figs. 1(d) and 1(e). This indicates the existence of stronger pinning cites along the ceiling and the bottom of the slab, and weaker pinning cites on the side wall of the slab. This is reasonable because the surface roughness of the ceiling and bottom is much larger than that of the side walls.

The observed planar defect should hold an almost dipole-locked structure because of the $R_T^2 \cong 1$. Figures 4(a) and 4(b) show the simplest almost dipole-locked structure which can form a planar defect in the y-z plane [20]. We call this structure a "dipole-locked soliton" (DLS). A domain of $(\hat{\boldsymbol{d}}, \hat{\boldsymbol{l}}) = (+\hat{\boldsymbol{y}}, +\hat{\boldsymbol{y}})$ is located on one side of the DLS, while the other domain of $(\hat{\boldsymbol{d}}, \hat{\boldsymbol{l}}) = (-\hat{\boldsymbol{y}}, -\hat{\boldsymbol{y}})$ is located on the other side of the DLS. In between, the two domains $\hat{\boldsymbol{d}}$ and $\hat{\boldsymbol{l}}$ are rotating their direction in the x-y plane, while keeping their parallelism except near the singularities, or the structure from $(+\hat{\boldsymbol{y}}, -\hat{\boldsymbol{y}})$ to $(-\hat{\boldsymbol{y}}, +\hat{\boldsymbol{y}})$ is equivalent. This structure cannot be stable in bulk. However, the DLS structure can be stabilized with a sacrifice of the energy for two line singularities on the surface of the wall, where the $\hat{\boldsymbol{l}}$ changes its direction from $+\hat{\boldsymbol{y}}$ to $-\hat{\boldsymbol{y}}$. The existence of such kind of singularity near the free surface of superfluid ^{3}He, namely, a surface chiral domain wall (SCDW), was suggested by Ikegami *et al.* [5] to explain their metastable intermediate data of electron transport in between two distinctive data under opposite uniform chirality. Similar SCDWs on the surface of sample cell walls contribute to stabilize DLS, as shown by the triangles in Fig. 4(a). The DLS has two narrow dipole potential wells near the singularities. The standing spin wave modes near the potential wells, whose R_T^2 are 0.94, 1.02, are shown in Figs. 4(c) and 4(d), respectively [20]. The spin wave amplitude for $R_T^2 = 0.94$ varies as an even function along the y axis with a little asymmetry, while the spin wave amplitude for $R_T^2 = 1.02$ varies as an odd function along the y axis. The little asymmetry in the former comes from a difference in texture near the two singularities. Because of the even-odd function nature of the two spin wave modes, the former mode couples to the NMR excitation field much stronger than the latter. These two modes could be coupled through a spin supercurrent to have a broader spectrum near $R_T^2 \cong 1$. The spatial size along the x axis of the DLS is determined by the thickness of the slab. This rather large size, and, namely, the slow variation of the dipole potential, leads to a higher value of R_T^2 compared to the dipole-unlocked soliton. The spatial width of the DLS in the MRI image is estimated to be 200 μm, which agrees reasonably well with a spatial distribution of the standing spin wave mode shown in Figs. 4(c) and 4(d).

The DLS and associated SCDWs form a chiral domain wall, whose NMR signature made it possible to experimentally visualize the spatial distribution of the chiral domain walls by our MRSI measurement. The observed chiral domain wall was identified as a dipole-locked soliton with the spectroscopic evidence. The domain had a macroscopic size of the order of 1 mm. Each adjacent domain should have an opposite chirality with each other. The domain structure appeared spontaneously during cooling through T_C and remained stable as long as the sample was kept quietly in temperatures far below T_C. Within our measurement, slow cooling through T_C was not effective in generating a monochiral domain structure. The domain

structure could be altered by the annealing process. Some flow generated by a thermal gradient in superfluid near T_C also showed an effect in altering the domain structure. However, we could not generate a monochiral domain among 40 independent coolings through T_C. It might be necessarily to introduce slow rotation while cooling through T_C as was shown by Bevan *et al.* [29]. The achievement represents a significant breakthrough not only for the study of chiral domain but also to visualize various topological objects in a topological superfluid, such as a spin-mass vortex [30], vortex sheet [31], and half-quantum vortex [32].

The authors would like to thank Masatomo Kanemoto for his contribution in the earlier stages of developing this experiment and the specialized MRSI method. This research was partially supported by MEXT KAKENHI Grant No. 23103509 and JSPS KAKENHI Grants No. 25103712 and No. JP15K13520.

*sasaki@scphys.kyoto-u.ac.jp

[1] D. Vollhardt and P. Wölfle, *The Superfluid Phases of Helium 3* (Taylor & Francis, London, 1990).

[2] G. E. Volovik, *The Universe in a Helium Droplet* (Clarendon Press, Oxford, 2003).

[3] P. M. Walmsley and A. I. Golov, Chirality of Superfluid ^{3}He-*A*, Phys. Rev. Lett. **109**, 215301 (2012).

[4] H. Ikegami, Y. Tsutsumi, and K. Kono, Chiral symmetry breaking in superfluid ^{3}He-*A*, Science **341**, 59 (2013).

[5] H. Ikegami, Y. Tsutsumi, and K. Kono, Observation of intrinsic magnus force and direct detection of chirality in superfluid ^{3}He-*A*, J. Phys. Soc. Jpn. **84**, 044602 (2015).

[6] V. F. Becerra and M. V. Milošević, Multichiral ground states in mesoscopic p-wave superconductors, Phys. Rev. B **94**, 184517 (2016).

[7] G. M. Luke, Y. Fudamoto, K. M. Kojima, M. I. Larkin, J. Merrin, B. Nachumi, Y. J. Uemura, Y. Maeno, Z. Q. Mao, Y. Mori, H. Nakamura, and M. Sigrist, Time-reversal symmetry-breaking superconductivity in Sr_2RuO_4, Nature (London) **394**, 558 (1998).

[8] F. Kidwingira, J. D. Strand, D. J. Van Harlingen, and Y. Maeno, Dynamical superconducting order parameter domains in Sr_2RuO_4, Science **314**, 1267 (2006).

[9] P. M. Walmsley, D. J. Cousins, and A. I. Golov, Critical Velocity of Continuous Vortex Nucleation in a Slab of Superfluid ^{3}He-*A*, Phys. Rev. Lett. **91**, 225301 (2003).

[10] P. M. Walmsley, I. J. White, and A. I. Golov, Intrinsic Pinning of Vorticity by Domain Walls of $\hat{\mathbf{l}}$ Texture in Superfluid ^{3}He-*A*, Phys. Rev. Lett. **93**, 195301 (2004).

[11] J. A. Sauls, Surface states, edge currents, and the angular momentum of chiral p-wave superfluids, Phys. Rev. B **84**, 214509 (2011).

[12] P. J. Hakonen, O. T. Ikkala, and S. T. Islander, Experiments on Vortices in Rotating Superfluid ^{3}He-*A*, Phys. Rev. Lett. **49**, 1258 (1982).

[13] P. J. Hakonen, O. T. Ikkala, S. T. Islander, O. V. Lounasmaa, and G. E. Volovik, NMR experiments on rotating superfluid ^{3}He-*A* and ^{3}He-*B* and their theoretical interpretation, J. Low Temp. Phys. **53**, 425 (1983).

[14] P. Hakonen, O. V. Lounasmaa, and J. Simola, Vortices in rotating superfluid ^{3}He, Physica (Amsterdam) **160B**, 1 (1989).

[15] Ü. Parts, J. M. Karimäki, J. H. Koivuniemi, M. Krusius, V. M. H. Ruutu, E. V. Thuneberg, and G. E. Volovik, Phase Diagram of Vortices in Superfluid ^{3}He-*A*, Phys. Rev. Lett. **75**, 3320 (1995).

[16] V. M. H. Ruutu, Ü. Parts, and M. Krusius, NMR signatures of topological objects in rotating superfluid ^{3}He-*A*, J. Low Temp. Phys. **103**, 331 (1996).

[17] V. B. Eltsov and M. Krusius, Topological Defects in ^{3}He Superfluids, in *Topological Defects and the Non-Equilibrium Dynamics of Symmetry Breaking Phase Transitions*, edited by Y. M. Bunkov and H. Godfrin (Kluwer Academic Publishers, Dordrecht, 2000), p. 325.

[18] C. M. Gould, T. J. Bartolac, and H. M. Bozlar, Experimental studies of solitons in superfluid ^{3}He-*A*, J. Low Temp. Phys. **39**, 291 (1980).

[19] Y. Sasaki, E. Hayata, T. Tanaka, H. Ito, and T. Mizusaki, Construction of ULT-MRI cryostat for ultra low temperature physics, J. Low Temp. Phys. **138**, 911 (2005).

[20] See Supplemental Material at http://link.aps.org/supplemental/10.1103/PhysRevLett.120.205301, which includes Refs. [21–24] to describe the experimental details, the method to extract the spectrum that originates from the defect, and a brief description of the numerical method to obtain the texture and standing spin wave mode.

[21] K. Sinokita, R. Toda, and Y. Sasaki, Construction of compact MRI magnet with superconducting shield, J. Phys. Conf. Ser. **150**, 012041 (2009).

[22] Y. Okamoto, M.Sc. thesis, Graduate School of Science, Kyoto University, 2016.

[23] R. Ishiguro, O. Ishikawa, M. Yamashita, Y. Sasaki, K. Fukuda, M. Kubota, H. Ishimoto, R. E. Packard, T. Takagi, T. Ohmi, and T. Mizusaki, Vortex Formation and Annihilation in Three Textures of Rotating Superfluid ^{3}He-*A*, Phys. Rev. Lett. **93**, 125301 (2004).

[24] T. Kunimatsu, H. Nema, R. Ishiguro, M. Kubota, T. Takagi, Y. Sasaki, and O. Ishikawa, Manipulating textures of rotating superfluid ^{3}He-*A* phase in a single narrow cylinder, Phys. Rev. B **90**, 214525 (2014).

[25] K. Maki and P. Kumar, Composite Magnetic Solitons in Superfluid ^{3}He-*A*, Phys. Rev. Lett. **38**, 557 (1977).

[26] K. Maki and P. Kumar, Composite solitons and magnetic resonances in superfluid ^{3}He-*A*, Phys. Rev. B **16**, 182 (1977).

[27] K. Maki and P. Kumar, Composite solitons and magnetic resonance in superfluid ^{3}He-*A*. II, Phys. Rev. B **17**, 1088 (1978).

[28] C. M. Gould and D. M. Lee, Double-Peaked Longitudinal and Transverse NMR Spectra in Superfluid ^{3}He-*A*, Phys. Rev. Lett. **37**, 1223 (1976).

[29] T. D. C. Bevan, A. J. Manninen, J. B. Cook, H. Alles, J. R. Hook, and H. E. Hall, Vortex mutual friction in superfluid ^{3}He, J. Low Temp. Phys. **109**, 423 (1997).

[30] Y. Kondo, J. S. Korhonen, M. Krusius, V. V. Dmitriev, E. V. Thuneberg, and G. E. Volovik, Combined spin-mass vortex with soliton tail in superfluid ^{3}He-*B*, Phys. Rev. Lett. **68**, 3331 (1992).

[31] Ü. Parts, E. V. Thuneberg, G. E. Volovik, J. H. Koivuniemi, V. M. H. Ruutu, M. Heinilä, J. M. Karimäki, and M. Krusius, Vortex sheet in rotating superfluid ^{3}He-*A*, Phys. Rev. Lett. **72**, 3839 (1994).

[32] S. Autti, V. V. Dmitriev, J. T. Mäkinen, A. A. Soldatov, G. E. Volovik, A. N. Yudin, V. V. Zavjalov, and V. B. Eltsov, Observation of Half-Quantum Vortices in Topological Superfluid ^{3}He, Phys. Rev. Lett. **117**, 255301 (2016).